We are IntechOpen,
the world's leading publisher of
Open Access books
Built by scientists, for scientists

4,800

Open access books available

122,000

International authors and editors

135M

Downloads

Our authors are among the

154

Countries delivered to

TOP 1%

most cited scientists

12.2%

Contributors from top 500 universities

WEB OF SCIENCE™

Selection of our books indexed in the Book Citation Index
in Web of Science™ Core Collection (BKCI)

Interested in publishing with us?
Contact book.department@intechopen.com

Numbers displayed above are based on latest data collected.
For more information visit www.intechopen.com

Microstructure – Hydro-Mechanical Property Relationship in Clay Dominant Soils

J. Gallier[1], P. Dudoignon[1] and J.-M. Hillaireau[2]
[1]HydrASA Laboratory, ENSIP, Poitiers University,
[2]INRA Domaine Expérimental,
France

1. Introduction

The hydro-mechanical properties of clay dominant soils are mainly governed by their clay mineral properties: i.e. mineralogy, interlayer charge, nature of exchangeable cations and associated swelling properties. The layer thickness of a clay mineral is usually measured by XRay Diffraction. Its responses to successive dry, hydration states and/or organic molecular saturation constitute the main tool for their identification (Brindley and Brown, 1980). The very great variety of these minerals is based on pure non swelling poles as kaolinite-serpentine, pyrophyllite-talc, illite–micas, chlorites and pure swelling poles as smectites. Besides these pure "end members" a lot of mixed layers as illite-smectite (I/S), kaolinite-smectite (K/S), chlorite-smectite (C/S) and many others can exist (Meunier, 2003; Brindley & Brown, 1980). These differences in mineralogy can induce differences in the hydro-mechanical properties of the clay matrices face to the shrinkage/swelling phenomenon (Tessier & Pedro, 1984; Tessier *et al.*, 1992). Consequently to the textural characteristics of the soil, they induce differences in the geotechnical properties from the weak plastic to very plastic and "liquid" domains according to the Atterberg classification. The relationships which can exist between the clay mineralogy and the hydro-mechanical properties of a soil do not depend directly of the mineralogical characteristics but mainly of the induced microstructure behaviour of these micro-divided clay media when submit to hydric or/and mechanical stress. Nevertheless, a low amount of smectite in a clay matrix assemblage can be sufficient to induce high swelling-shrinkage properties (Bernard, 2006; Bernard *et al.*, 2007). Biarez *et al.* (1987) demonstrated the similitude of the state path of a kaolinitic matrix during compression by oedometer test and during desiccation: the suction pressures induced during the desiccation cycle may be compared to the compression pressures applied during the compressibility test. The clay matrix microstructure behaviours may be represented along their shrinkage curve in volume/ water content (V-W) diagram or in "normalized" void ratio – water content (e-W) diagram. At a macroscopic scale the pedologists commonly reconstruct the soil shrinkage curves by rehydration of unremoulded but dried soil samples (Braudeau *et al.*, 1999; 2004). The method allows a characterisation of the macro-porosity of the sampled soils for accurate depths. On another way, the shrinkage curve can be obtained on the clay matrix in order to characterize the micro-arrangement of clay particles (Bernard, 2006; Bernard *et al.*, 2007).

In fact hydro-mechanical properties of a clay dominant material have to be studied at successive scales from the crystallite size to the macroscopic scale. Thus, the characterization from the microstructure-to-macroscopic scale is one of the main topic face to the explanation and model of the clay dominant material behaviours in civil engineering, pedology and soil farming domains. Many tools are currently used to measure the hydro-mechanical properties of soils. They can be "*in situ*" investigations as penetrometer, scissometer and pressiometer for mechanical parameters and "infiltration" tests for hydraulic conductivity. They can also be laboratory measurements by scissometer, triaxial cell or oedometer. All these techniques of investigation give whole characteristics of the material at the macroscopic scale.

The topic of this chapter is to propose a methodology for macroscopic-to-microscopic scale switch. The switch method is based on the use of the clay matrix shrinkage curve as tool for:

1. the calculation of numeric relationships between macroscopic "*in situ*" or laboratory measurements and the clay matrix microstructure (Perdok *et al.*, 2002; Bernard *et al.*, 2007; Bernard-Ubertosi *et al.*, 2009).
2. the modelling of the shrinkage-swelling phenomenon in the structural evolution of soils (Gallier, 2011).
3. The calculation of numeric relationship between the soil resistivity and the microstructure.

The method was induced by previous works on the clay matrix microstructure behaviours based on image analyses of thin sections captured by optical microscopy and by SEM (Dudoignon & Pantet, 1998; Dudoignon *et al.*, 2004; Dudoignon *et al.*, 2007).

The investigations were made on clay-rich soils of marsh (Atlantic coast of France). The "*in situ*" investigations consist in parallel profiles of cone resistance (Qd; dynamic penetrometer), shear strength (C; scissometer), soil resistivity (ρs; salinometer). They are coupled with water content (W) and density profiles plus 1/5 soil conductivity profiles (CE$_{1/5}$) measured on soil samples (Pons, 1997; Pons & Gerbeau, 2005).

2. Material and methods

Face to the dependence of the hydro-mechanical properties of soils on their texture and mineralogy, the studies, focussed on the mechanisms and model of clay dominant soil behaviours, require investigations on textural and mineralogical homogeneous clay material. For that, the experimental sites studied are located in the Marsh of Rochefort which belongs to the West Marsh located along the Atlantic coast of France (Figure 1a). The material consists in clay-rich soils formed by desiccation and consolidation of fluviomarine sediments which have shown:

1. their textural and mineralogical homogeneity all over the West Marsh area (Ducloux, 1989; Righi *et al.*, 1995; Pons & Gerbaud, 2005; Bernard, 2006),
2. and structural profiles which show the clay-rich material from its solid state near the surface down to plastic and liquid state in depth (Bernard, 2006. Bernard *et al.*, 2007; Bernard-Ubertosi *et al.*, 2009; Dudoignon *et al.*,2007 ; 2009 ; Figure 1b).

2.1 Geological setting

The "Marais Poitevin", the "Marais Breton-Vendéen" and the Marsh of Rochefort are the three largest marshes of the French Atlantic Coast. For this work the "*in situ*" investigations were performed in the "Marais Poitevin" and then focused on the experimental site of the INRA of St Laurent de la Prée in the Marsh of Rochefort (Figure 1a; Bernard, 2006; Gallier, 2011). The soils result from the surface desiccation and consolidation of the clay-rich fluviomarine sediments (Bri) dated of the Flandrian transgression.

The age of sediments ranges from 10 000 years BP to the present. The soil formation results mainly from the reclaiming of land from the sea by polders since the Middle Ages and consequently from compaction and maturation of salt-marsh mud. The Bri is characterized by a fine-grained texture (85-to-92% of particles < 20 μm) and small organic matter content (0.4 to 2.4%). The Cationic Exchange Capacity of the material range between 20 and 30 meq/100g. These are C.E.C. according to the "illite domain". In fact the X Ray diffractions identify the Bri clay matrix as an assemblage of dominant illite plus kaolinite and illite/smectite mixed layers and very small amount of pure smectite. The micro-chemical analyses of the assemblage spread from the illite domain to I/S domain in the M^+, $4Si$, $3R^{2+}$ Meunier's triangle (Bernard, 2006; Dudoignon *et al.*, 2009). The mineralogy is homogeneous all over the different studied sites. One can remarks only a weak increase of the smectitic layers % of the I/S with depth in the < 0.2 μm fraction. These minor mineralogical evolutions cannot imply realistic changes in the hydro-mechanical behaviour of the Bri (Bernard, 2006). The shrinkage, plasticity and liquidity limits are 20%, 40% and 70% in weight % respectively.

The structural profiles of the soil are governed by the desiccation mechanism which operates from the surface to the depth. The consequence is an increase of the water contents from the surface to the depth during the dried seasons. The hydric state of the material evolves from the shrinkage limit in surface down to the plasticity limit and liquidity limit in depth (Figures 1 and 2). The hydric state of the clay material is characterized by its water content (W), its associated wet density (γw) and its void ratio (e). Thus the structural profiles may be represented in the e-W diagram where they superimposed on the shrinkage curve of the clay matrix constituting the Bri (Figure 2b). The hydraulic management of the marshes area divides the territory in dried marsh locate in the central part of the territory and wet marshes located along the peripheral limestone – Bri contact. The role of the wet marsh is the storage of fresh water during winter.

2.2 Methods

The topic of the work is to record in parallel vertical profiles of physical and mechanical characteristics: water content (W), wet density (γw), cone resistance (Qd), shear strength (C), 1/5 soil electrical conductivity ($CE_{1/5}$) and "*in situ*" soil resistivity (ρs). The physical parameters (W, γw, $CE_{1/5}$) were measured from the surface to 2.00 m depth on samples cored using a clay-auger, the mechanical parameter (Qq, C), and soil resistivity (ρs) were obtained by "*in situ*" investigations.

The water content is calculated in weight % by difference between the "*in situ*" wet sample mass and 105°C (24 hours) dried mass referring to the dried mass. The density is measured by double weighing after paraffin coating. The porosity (n) and void ratio (e) are calculated as follows:
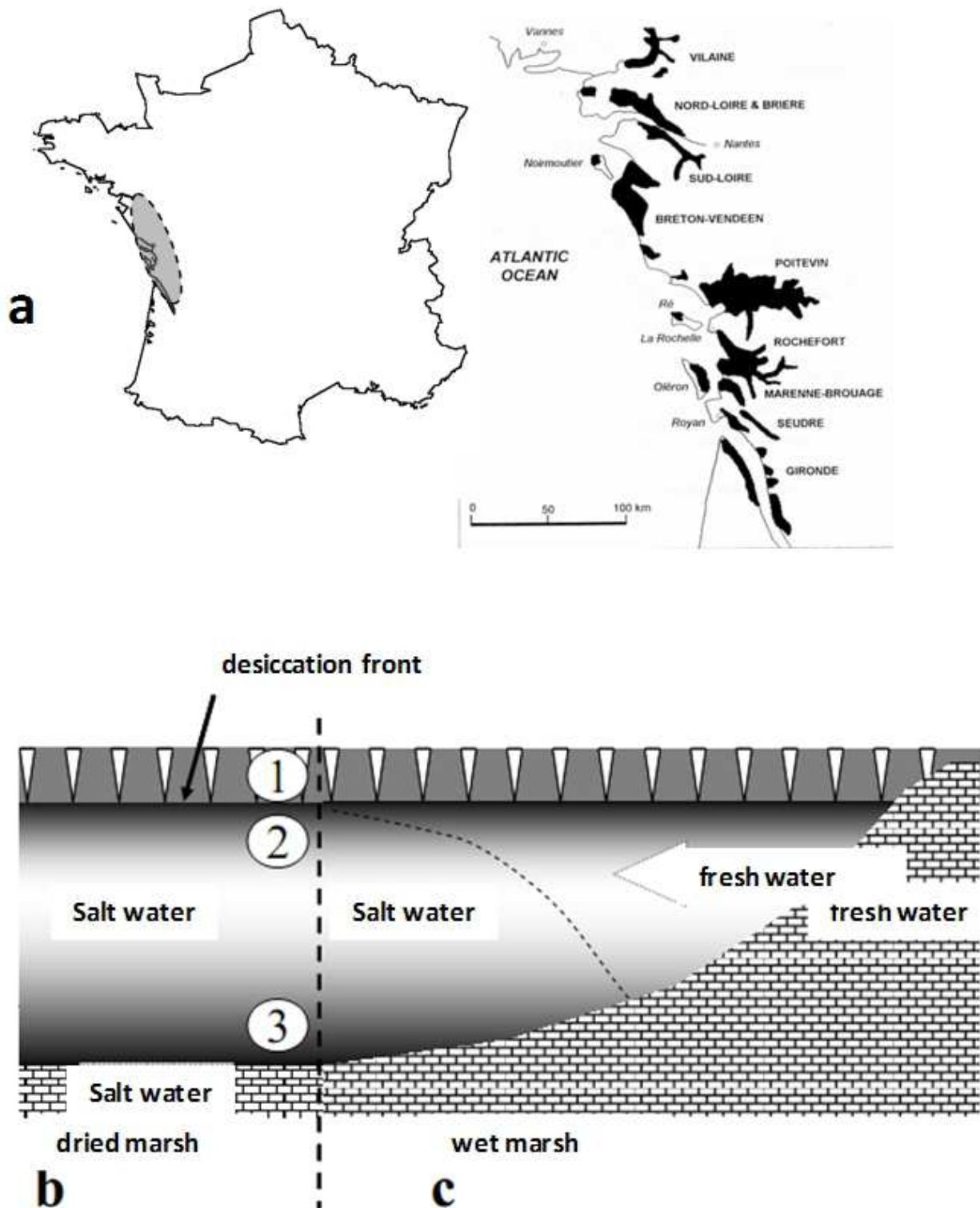
Fig. 1. a- Location of the West marshes and Mash of Rochefort along the West altlantic coast of France. b & c schematic representation of the sediment-to-soil structure evolution overlapping the limestone.(1 desiccated and consolidated soil in solid state; 2 – plastic state, 3 – liquid state).b - The Bri is saturated by fossil salt water in the dried marsh. c - It shows fresh water inlet from the peripheral limestone hills in the wet marsh.

$$n = \frac{Vv}{Vt} = \frac{Vt - \frac{Md}{\delta s}}{Vt} \quad (1)$$

and

$$e = Vv/Vs = \frac{n}{n-1} \quad (2)$$

where V_v (cm³) is the void volume (air + water), V_t is the total sample volume, Vs the solid volume, Md is the dried sample mass (g), γs is the average mineral density measured using pycnometer. It is equal to 2.58 g/cm³.
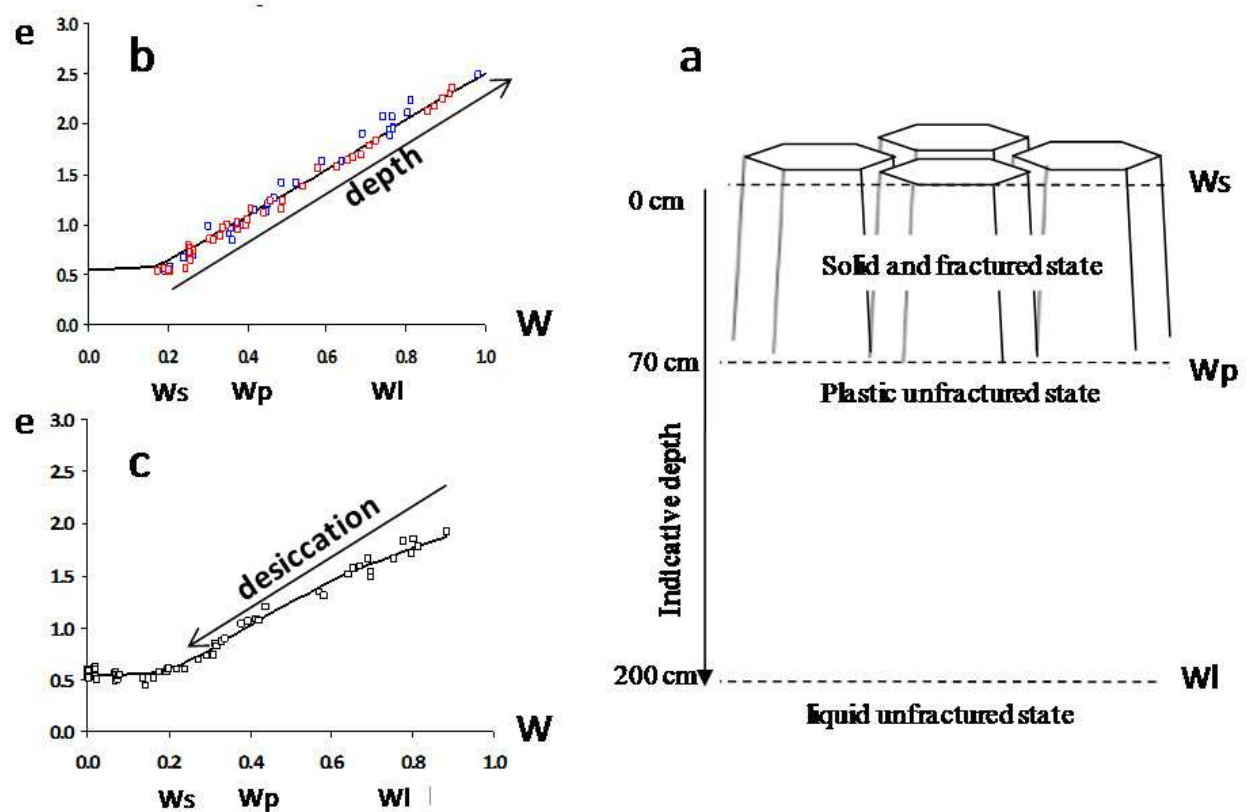

Fig. 2. The structural evolution of the clay dominant soil may be represented by the (e-W) shrinkage curve of the clay matrix, a – schematic representation of the structural profile, b-representation of the W profiles in the e-W diagram, c - clay matrix shrinkage curve obtained by drying of initial unremoulded samples. Ws = shrinkage limit, Wp = plasticity limit, Wl = liquidity limit, e = void ratio, W = gravimetric water content

The cone resistances were measured using a PANDA dynamic penetrometer with variable energy. It is a light apparatus particularly well adapted for these wetlands (Bernard et al., 2007; Bernard-Ubertosi *et al.*, 2009). The method and its relations to other *"in situ"* measurements were described by Gourvés & Barjot (1995) and Langton (1999). The cone is driven into the soil using a fixed-weight hammer and the dynamic cone resistance is calculated by a microprocessor for each penetration (< 4 cm) following the so-called "Dutch Formula" (Cassan, 1988; Zhou, 1997):

$$Qd = \frac{MV^2}{2Ad} * \frac{1}{1+\frac{P}{M}} \tag{3}$$

with d the penetration (cm), M the weight of the striking mass (kg), P is weight of the struck mass (rod +cone; kg), V is the impact velocity (cm^{-1}), Qd is the cone resistance (MPa), and A is the cone section (cm^2). In these marshlands, lost cones of 4 cm^2 section (2 cm^2 rod section) have been used in order to avoid the artifact of rod-clay contact.

The shear strength was measured using a GEONOR H-70 field vane shear test. Three sizes of four-bladed vanes are used for a total range of 0-260 kPa: 16 mm (total width of two opposite blades) * 32 mm (blade height), 20*40 mm and 25.4*50.8 mm. The precision of the measurement is ± 1 kPa.

The hydraulic conductivity is measured on test pieces of Bri during oedometer compressibility tests. The experiments were performed on unremoulded core-samples around 2 m depth in saturated state near the liquidity limit. The successive steps of consolidation allow successive measurements of the hydraulic conductivity for a decrease of the void ratio from 2 (equivalent to Wl) to 0.5 (equivalent to Ws; Figures 3, 13).
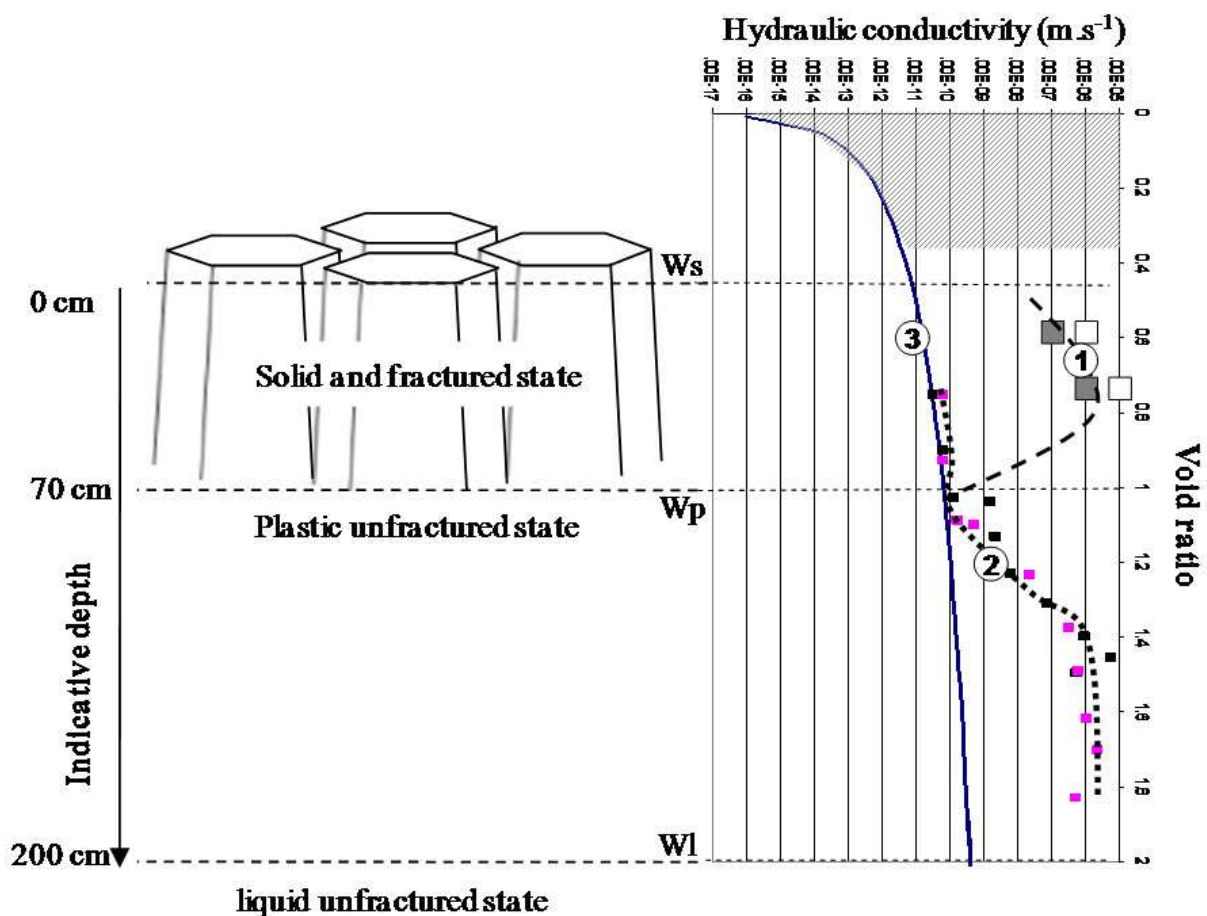

Fig. 3. Representation of the vertical evolution of the Bri structure and soil hydraulic conductivity; 1 (large squares) "*in situ*" infiltrometry measurement in the fractured surface layer (unsaturated solid state), 2 (small squares) oedometer measurement on saturated and unfractured clay material, 3 (continuous line) theoretical profile of hydraulic conductivity based on the microstructural parameters. The dashed domain does not exist "*in situ*".

The microstructure – hydro-mechanical properties relationships were demonstrated by the petrographic studies of consolidated and sheared kaolinitic test pieces using a triaxial press (Dudoignon et al., 2004). The state ways of the simple consolidated or over-consolidated and sheared clay matrix have been represented in a Cam-clay type diagram (e versus log P). In the same time, the hydraulic conductivities of the damaged clay matrices were calculated using a Kozeny-Carman equation which took into account the micro-structure parameters as porosity, surface area of clay particles and tortuosity of the matrix (Grolier *et al.*, 1991; Dudoignon *et al.*, 2004):

$$K = \left(\frac{1}{2T^2}\right)\left(\frac{n^3}{Ssp^2}\right) \tag{4}$$

with Ssp= S (1-n) with S = particle surface area = specific surface / volume, T = tortuosity, n = porosity.

For the Bri, the clay matrix hydraulic conductivities are calculated using the specific surface of the clay particles (60 m²/g) calculated from the laser granulometry. The porosity (n) is calculated for each equivalent void ratio (e). To simplify, the tortuosity was calculated for average 2-5 shape factor of particles and for an isotropic medium. In the 0.5 – 2.0 void ratio range, the tortuosity evolves from 1.28 to 1.80 (Dudoignon *et al.*, 2004; 2009).

3. Results

3.1 Gravimetric water content profiles and clay matrix shrinkage curve

The switch from gravimetric water profile to shrinkage curve is based on the calculation of the void ratio (e) for each W measurement. The e calculation needs the measurement of the sample wet density (γw) associated to each W measurement. The void ratio is calculated as follows:

$$e = \frac{\gamma s - \gamma d}{\gamma d} \tag{5}$$

with:

$$\gamma d = \gamma w/(1 + W) \tag{6}$$

γs = particle density, γw = wet sample density, γd = dried sample density, W=gravimetric water content, e= void ratio.

The presented results were obtained on the INRA experimental site of St Laurent de la Prée on grassland and cultivated field. In these marshlands, whatever the investigation site, the general soil profile shows an increase of the water content from the surface to the depth and consequently associated decrease of γw and γd (Figures 2 & 4).

The shrinkage curve can be calculated from these *"in situ"* data: i.e. e calculation from W and γw measurements. It shows the soil structure evolution in the Ws – Wl domain which is observed *"in situ"*. From Wl to Ws the curve shows the void ratio decrease from 2.0 down to 0.55, and for W < Ws the void ratio is constant (e = 0.55). The shrinkage curve can be approached using the Cornelis equation (Cornelis *et al.*, 2006; Figure 2b):

$$e = e_0 + \gamma(\exp(-\frac{\xi}{9^{\xi}}) \tag{7}$$

with $e_0 = 0.55$, $\gamma = 11.59$, $\xi = 1.78$, $\vartheta = W$, $\zeta = 0.63$.
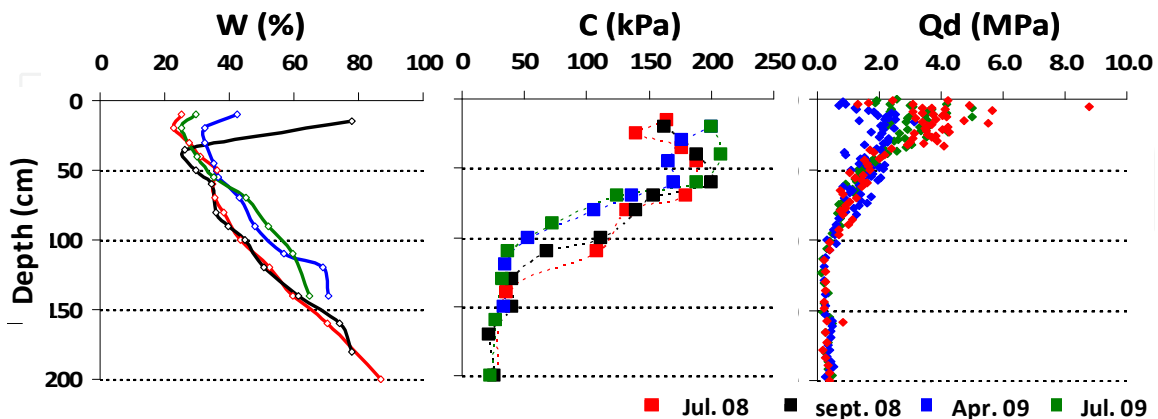

Fig. 4. Example of water content (W), shear strength (C) and cone resistance (Qd) profiles recorded in the grassland in July 2008, September 2008, April 2009 and July 2010.

The shrinkage curve has been also obtained in laboratory by drying unremoulded samples of Bri at initial water contents near the liquidity limit. The shrinkage curve has been constructed step by step from daily density and gravimetric water measurements during the drying phases up to the full desiccation at 105°C (Bernard *et al.*, 2007). This "laboratory" curve differs from the "*in situ*" one by a weak curvature in the 0.5 – 0.9 W domain (Figure 2b & c). Nevertheless, it can be modelled by a second Cornelis equation with $e_0 = 0.55$, $\gamma = 2.47$, $\xi = 0.54$, and $\zeta = 1.23$. From W= 0 to W=0.50 these two shrinkage curves are perfectly superimposed. Bernard *et al.* (2007) demonstrated that the shrinkage is isotropic in the Ws - Wp domain. In fact, all the structural profiles recorded in the marsh territories, are well superimposed on the "*in situ*" shrinkage curve. The slope of the shrinkage curve is equal to the average particle density (2.58 g/cm³) measured by pycnometer (Bernard, 2006; Gallier, 2011).

This "*in situ*" shrinkage curve of the clay matrix is used as reference in the following works. It has the role of tool to establish the structure-to-hydro-mechanic relationship for these marsh soils.

3.2 Mechanical resistance profiles

3.2.1 Cone resistance and shear stress profiles

The "*in situ*" penetrometer profiles were driven down to 2 m depth in grassland (Figure 4) and in the cultivated field (Figure 5). The Qd are measured by steps of 1-to-4 cm. From the surface to the depth, the Qd profiles cross through (1) the clay material in solid state, for depths equivalent to the Ws-Wp domain, (2) the clay material in plastic state (Wp – Wl domain), and (3) the clay material in liquid state for W > Wl (Figures 4 & 5).
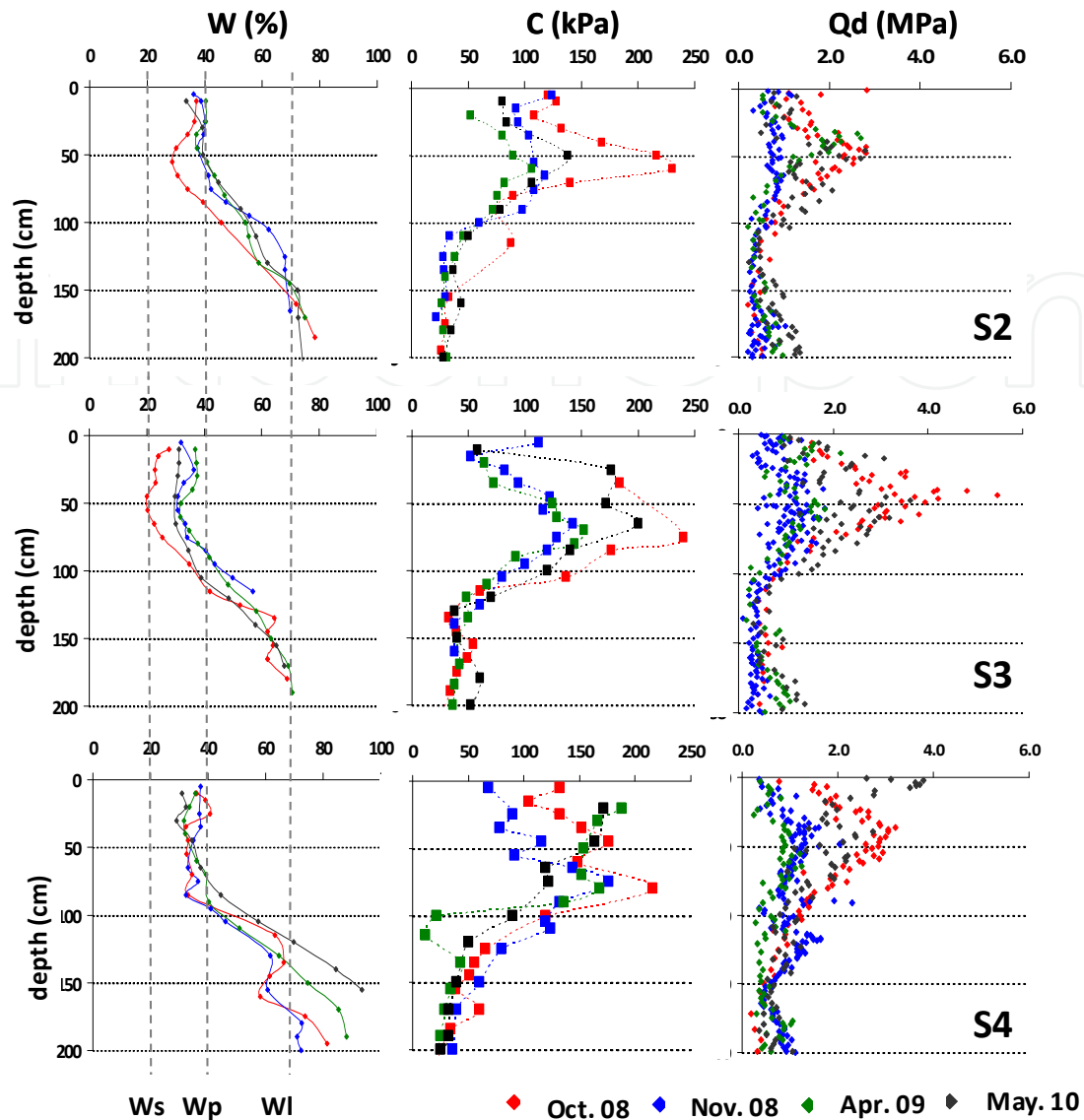
Fig. 5. Example of water content (W), shear strength (C) and cone resistance (Qd) profiles recorded in the S2, S3 and S4 sites of the corn-field in October, November 2008, April 2009 and May 2010.

The cone resistance (Qd) depends of the structure of the clay material and of its consolidation state. Thus, in the objective to get soil structure-mechanical properties relationships, the idea was to measure the Qd profiles parallel to the desiccation profiles. In fact, the successive investigations shown that the Qd profiles are able to record the desiccation effects but also superimposed structural evolutions of surface due to the tillage or other farming works plus structural evolutions in depth due to the soil over-consolidation in paleosol levels (Bernard *et al.*, 2007; Gallier, 2011). In order to get numerical W-e-Qd relationship with realistic correlation factors the following work was focused on soil profiles exempt of tillage zone or paleosol. The Qd profiles show vertical evolutions which are symmetric to the W profiles. According to the weak W values of surface, they present a Qd peak from the surface to the depth of 50 cm. The Qd peak maximum increases according to the desiccation intensity. From 50 cm to 100-120 cm they show a progressive

decrease of the Qd values until the inferior limit of measurement. From 100 cm to 200 cm the Qd values are very weak and constant whatever the season. These three vertical domains accord with the superimposition of the solid state (0-50 cm), solid-to-plastic state (50-100 cm) and plastic-to-liquid state (100 cm – 200 cm) (Figure 4 & 5).

The *"in situ"* shear strength (C) profiles where also driven down to 200 cm deep but by steps of 10 cm according to the clay auger sampling.

The main differences between the Qd and C measurement are due to the soil-tool interactions (Figure 6):

- a volumetric deformation and compression of the soil around the penetrometer cone
- a shearing of soil along a cylindrical surface during the shear test
- a very short time of soil damaging (few milliseconds) due to the hammer impact of the penetrometer
- a slow rotation of the shear vane for the shearing test.

Nevertheless, the vertical evolutions of the C profiles are similar to the Qd profiles: high C values for high desiccation of surface and low values for depths > 100 cm (Figures 4 & 5).
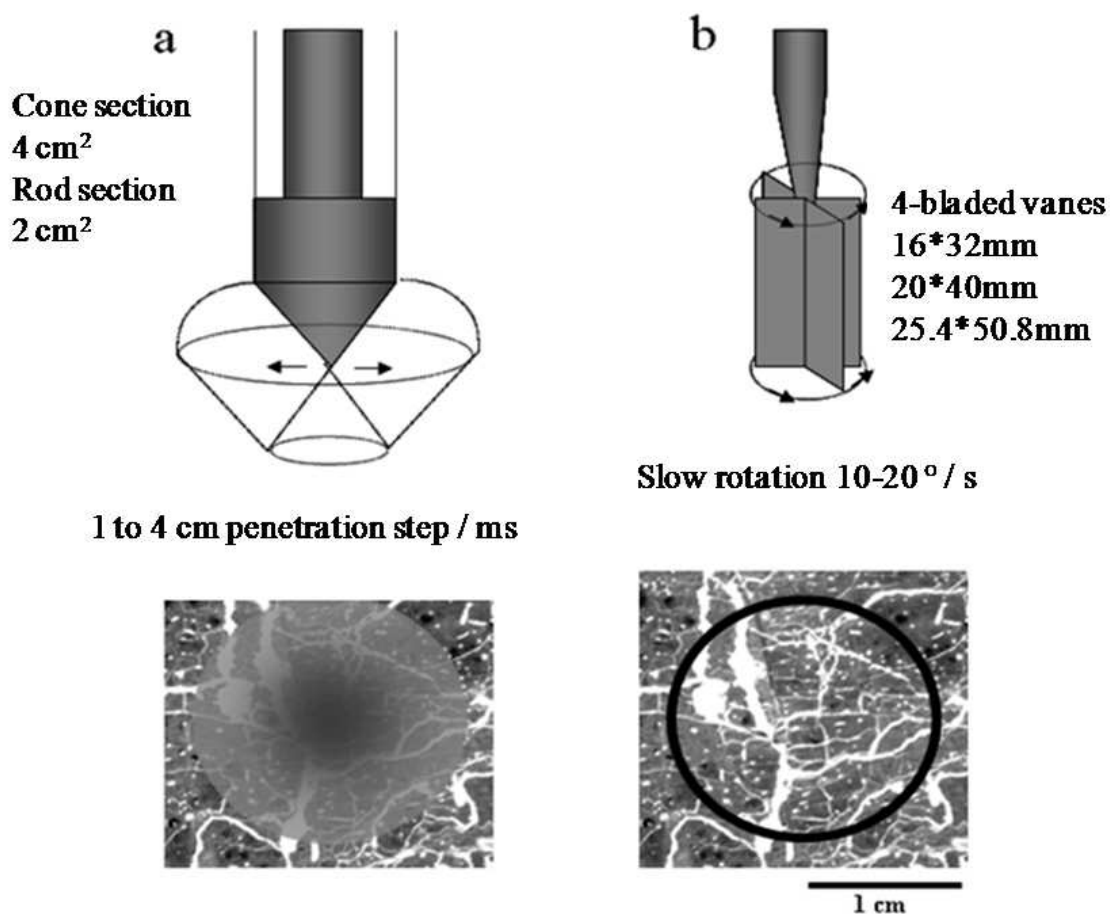

Fig. 6. Schematic representation of the impacts of the penetrometer cone and shear vanes on the soil structure. Soil photographies are grey level image of polished section. White = macroporosity and shrinkage fractures, grey = clay matrix.

3.2.2 Cone resistance and shear strength profiles – Structural profile relationship

The structural evolution of the soil from the surface to the depth may be represented by the clay matrix shrinkage curve. Thus the C and Qd profiles – W profiles relationship may be represented in a W-e-Qd or C diagram. In the e-Qd and e-C diagram the Qd and C profiles describe an hyperbolic like curve with two asymptotic ends: drastic increase of Qd an C values for low e values (desiccated and consolidated surface layer) and very low values in the plastic-to-liquid domain (Figure 7).
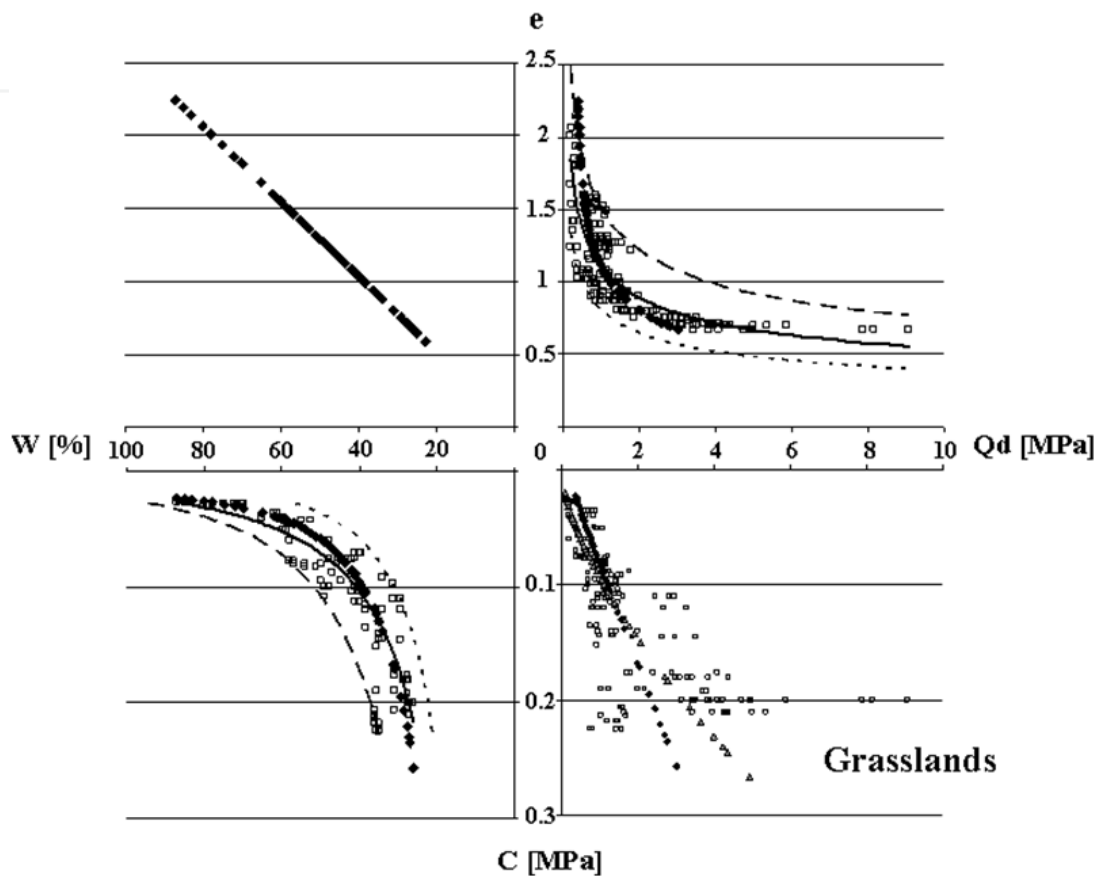

Fig. 7. Representation of the shrinkage curve – Qd and C profiles in the W-e-Qd-C crossed diagram. Example of the grassland (black line = power law equation; black lozenges = Perdok's like equation, dashed lines = limits of the domain by power law equations).

Two types of equation can model the Qd and C profiles taking into account the W or e values:

- the Perdok modified equation (Perdok *et al*. 2002; Bernard-Ubertosi *et al.,* 2009; Gallier, 2011)
- and power law equation (Gallier, 2011)

The Perdok equation is written as follows (for Qd or C):

$$\log (Qd) = a_0 + a_1 \frac{e}{1+e} + W (a_2 + a_3 \frac{e}{1+e}) \tag{8}$$

$$\log (C) = a'_0 + a'_1 \frac{e}{1+e} + W (a'_2 + a'_3 \frac{e}{1+e}) \tag{9}$$

The a_0, a_1, a_2 and a_3 Perdok's coefficients have to be fitted to minimize the sum of absolute values of the differences between measured and calculated data.

The power law is as follows (for Qd or C):

$$Qd = (e/A)^{1/b} \text{ or } Qd = (\gamma sW/A)^{1/b} \tag{10}$$

$$C = (e/A')^{1/b'} \text{ or } C = (\gamma sW/A')^{1/b'} \tag{11}$$

with A and b calculated to minimize the sum of absolute values of the differences between measured and calculated data.

The power law equation is easy to use which A and b coefficients which present weak variations between the successive runs and with A an b roles which are clearly identified on the vertical shift of the curve and on the curve shape. The Perdok's equation present some drawbacks due to the disparities between the a_0, a_1, a_2 and a_3 coefficients for different runs and lack of understanding on the roles of each parameter on the curve location and shape (Table 1).

	Qd profiles					
	Perdok's equation				Power law	
	a_0	a_1	a_2	a_3	A	b
grassland	2.89	-5.56	-0.76	1.39	1.1	-0.29
Bernard (2006)	2.34	-5.20	0.74	0.34		
cornfield	-0.35	5.68	-9.28	6.24	1.14	-0.42
	C profiles					
	Perdok's equation				Power law	
	a'_0	a'_1	a'_2	a'_3	A'	b'
grassland	-3.36	8.08	1.37	-10.39	0.44	-0.40
cornfield	1.64	-4.93	-2.08	3.35	0.36	-0.48

Table 1. Recapitulative table of Perdok's a_0, a_1, a_2, a_3 parameters and A and b power law parameters for the Qd and C profiles.

3.3 "In situ" resistivity profiles and soil electrical conductivity

3.3.1 "In situ" resistivity

The "*in situ*" soil resistivity was measured following two methods:

- vertical resistivity (ρs) profiles using a penetrometer-salinometer coupling (Bernard-Ubertosi *et al.*, 2009)
- and vertical resistivity sections (Bernard, 2006; Gallier, 2011).

The penetrometer-salinometer coupling consists in driving the salinometer in the penetrometer hole after the Qd measurements. The method has the advantage to give real resistivities at measured depths (Bernard-Ubertosi et al., 2009). It has the drawback to be limited in depth. The used resistivimeter is a Syscal R1+. The salinometer device is a A-M-N-B Wenner type with 3 cm AM, MN and NB apart.

The resistivity sections are recorded following Wenner-Schlumbeger configurations. They are inverse calculated according to the apparent measured resistivity and need to be standardized. The used resistivimeter is a Syscal R1+ interfaced with a 48 electrodes switch. The measurement sequences are loaded via the ELECTRE II software. The data are transferred to a PC with the PROSYS software. The resistivity sections are calculated with RES2DINV software (Figure 8).
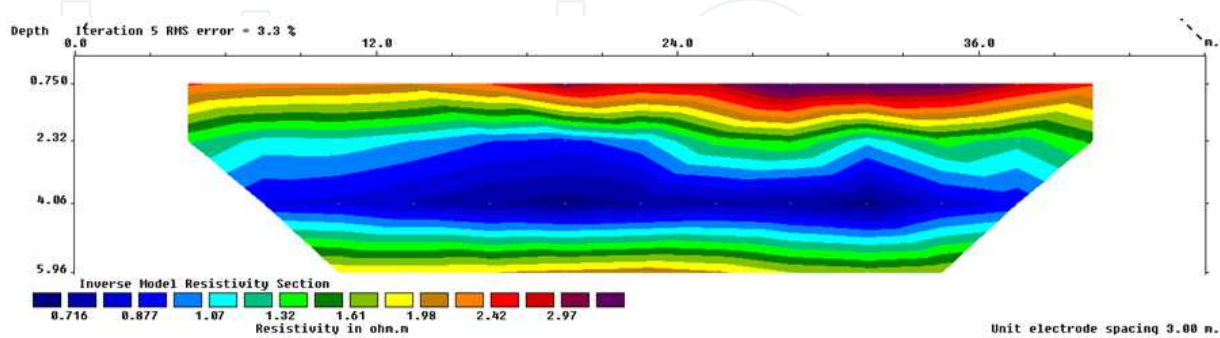

Fig. 8. Example of resistivity section showing the vertical structure of the Bri with high resistivity representative of the dried and consolidation surface level (solid state), intermediate resistivity characteristic of the plastic state and lowest resistivity around 4 meter depths for the Bri in liquid state and salt water saturated (grassland).

The parallel recording of W and ρs have allowed the fit of the Archie's law (1942) for these clay-dominant soils. Following the Archie's law the soil resistivity depends of the porosity (ϕ), saturation index (sat) and fluid resistivity (ρf):

$$\rho s = \alpha \, \rho f \, \phi^{-m} Sat^{-n} \tag{12}$$

with α=formation factor, m = cementation factor, n = factor characteristic of the medium.

The water content – resistivity profiles relationship had hollowed the calculation of an equivalent Archie's equation for our marsh soils (Bernard-Ubertosi *et al.*, 2009; Gallier, 2011; Figure 9):

$$\rho s = 1.01 \, \rho f \, \phi^{-2.73} Sat^{-2} \tag{13}$$

In fact the resistivity of a clay rich soil depends of the electrolytic conductivity and the mineral surface conductivity. Thus the initial Archie's law only valid for unclayed rocks have to take into account the clay nature of minerals by their C.E.C (Waxman & Smits, 1968).

The Waxman & Smits' equation takes into account the clay mineral C.E.C as follows:

$$\rho s = \frac{Sat^n}{a \, \phi^{-m}} \left(\rho f + \frac{B \, Qv}{Sat} \right) \tag{14}$$

with a = factor dependant of the medium, Qv = CEC, and B = parameter representative of the mobility of the exchangeable cations of the clay structures. The B parameter can be calculated as follows (Mojid & Cho, 2008):

$$B = 4.78 \, 10^{-8} \, \left(1 - \exp\left(\frac{-\rho f}{0.013} \right) \right) \tag{15}$$

The Waxman & Smits calculations made with a average 25 meq/100g CEC and fluid conductivities measured on water sampled in piezometers (2 S.m^{-1} and 4 S.m^{-1} in corn field and grassland respectively) give results equivalent to the resistivities calculated following the simple Archie's law. In these salt media of coast marshes, the high fluid conductivities minimize the clay mineral surface effect.

Once more the clay matrix shrinkage curve can be used as tool for the representation of the structure-resistivity relationship in our marsh soil environment (Figure 9)
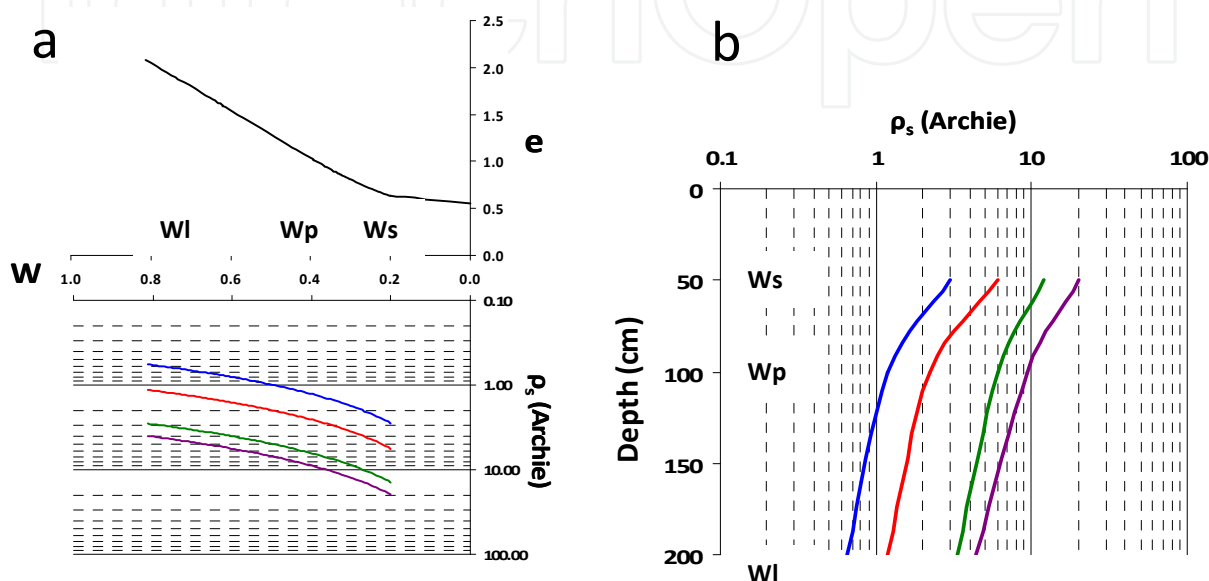
Fig. 9. Soil resistivity – shrinkage curve relationship. a- The W or e – resistivity curves are calculated in the Wr-Wp saturation domain using the Archie's law. The vertical shift of the ρs curves is due to the fluid salinity (calculations for 0.2, 0.4, 1.0, and 1.4 Ω.m). b - Equivalent vertical ρs profiles; the horizontal shift is due to the fluid salinity.

3.3.2 Electrical conductivity of soils

The "*in situ*" resistivity measurements are based on the role of porosity, saturation index and fluid resistivity. The resistivity – shrinkage curve relationship is based on the homogeneity of the fluid resistivity (Figure 9). In the marsh territories the soil properties evolve following two major mechanisms: (1) the descending progression of the desiccation fronts and (2) the fresh water – salt water exchange. The geo-electrical investigations are able to indicate the evolution of fluid salinity in soil but are not sufficiently detailed to allow realistic inverse calculation of structure –salinity-resistivity.

For this reason, profiles of 1/5 Electrical Conductivity (CE$_{1/5}$) of soils were measured. The measurements were made on soils sampled from the surface to 2.00 m depth every 10 cm, according to the clay auger sampling for water profiles. The C.E.$_{1/5}$ were measured on 1/5 extracts (10 g of dried soil in 50 g of distilled water; Pons & Gerbaud, 2005). The "*in situ*" soil electrical conductivity values depend of the water content, fluid chemical composition, soil mineralogy and the soil structure. In fact, the CE$_{1/5}$ measurements are made from 10g of dried soil, thus the CE$_{1/5}$ is "independent" from the soil water content. Nevertheless it is possible to calculate the fluid conductivity (CEf) following the Montoroi (1997) formulae:

$$CEf = CE_{1/5} \, (5W) \tag{16}$$

with CEf= the *"in situ"* fluid conductivity, $CE_{1/5}$ the soil conductivity measured in laboratory and W the gravimetric water content (Figure 10).
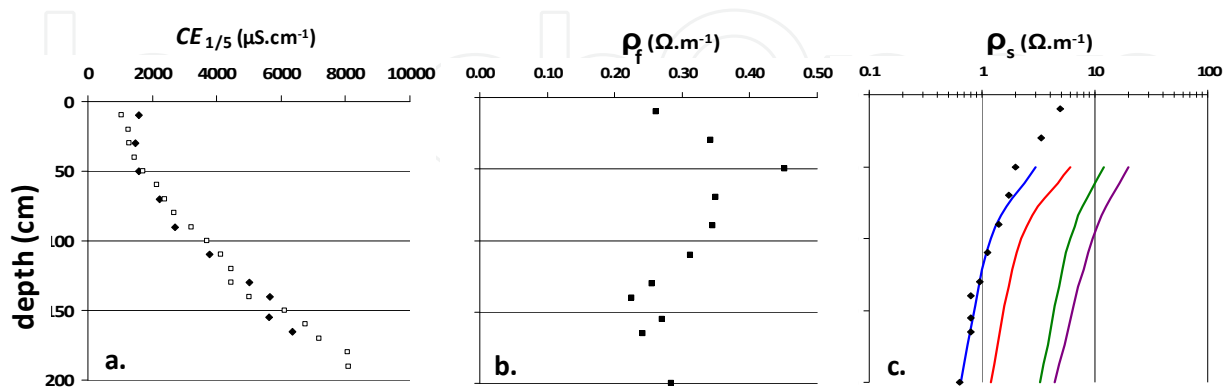

Fig. 10. Example of fluid resistivity profile (ρ_f) and soil resistivity (ρ_s) profiles calculated in the grassland from the $CE_{1/5}$ and W profiles and using the Montoroi relation plus the Archie's law. The inverse calculated profile (black points) of resistivity is well superimposed on the theoretical profile calculated with the Archie's law with a 0.2 Ω.m resistivity of salt fluid.

In the corn field the $CE_{1/5}$ profiles were recorded in September 2006, April 2007, December 2007and June 2008. For each site and whatever the date, the $CE_{1/5}$ profiles are quite superimposed (Figure 11). They are governed by the inter-seasonal water sheet level evolution and mainly by the thickness of leached soil. The $CE_{1/5}$ profile shapes evolve following the site locations:

- Progressive evolution from the surface to the depth along the southern part of the field. This southern part is located against the limestone hill which induces fresh water inlet into the Bri.
- Deep leached zone and drastic $CE_{1/5}$ increase in depth in the northern part of the field which is characterized by very low water level.

The CEf profiles calculated from the $CE_{1/5}$ and W profiles allow the calculation of the associated soil resistivity profiles which clearly show the vertical evolution due to the fresh plus salt water mixture along the limestone contact or due to the leaching of unsaturated upper level (Figure 12).

4. Discussion and soil structure – Hydromecanical property relationships

The mineralogical and textural "homogeneities" are characteristics of the clay dominant soils of our marshes which have been developed by polders on fluvio-marine sediments. A second advantage is the vertical evolution of the clay material from its solid state in surface
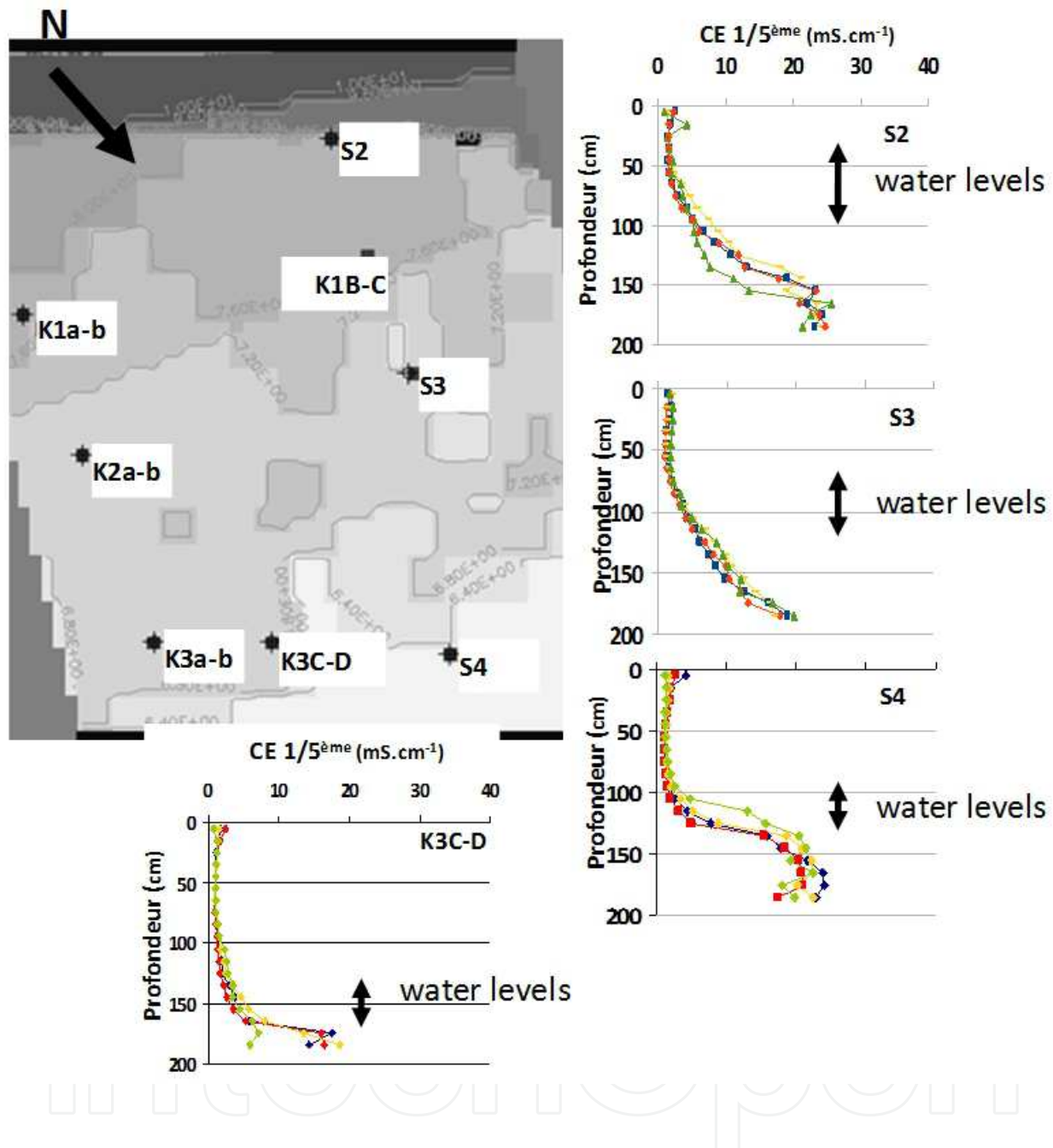
Fig. 11. Example of the $CE_{1/5}$ profile evolutions in the corn field with indication of inter-seasonal water level evolution. S2 to S4 and K1 to K3 are locations of the piezometers.

to a plastic and a liquid state in depth. In these conditions the studied marsh soils allow the transposition water content profiles– clay matrix shrinkage curve. Using the shrinkage curve the mechanical properties (Qd & C) – structure relationships may be written following power law or Perdok's like equations (Figure 13). The soil resistivity – structure relationship is an Archie's law and the hydraulic conductivity of the clay matrix may be directly linked to the shrinkage curve via experimental measurements (Figures 9, 10, 12 and 13).
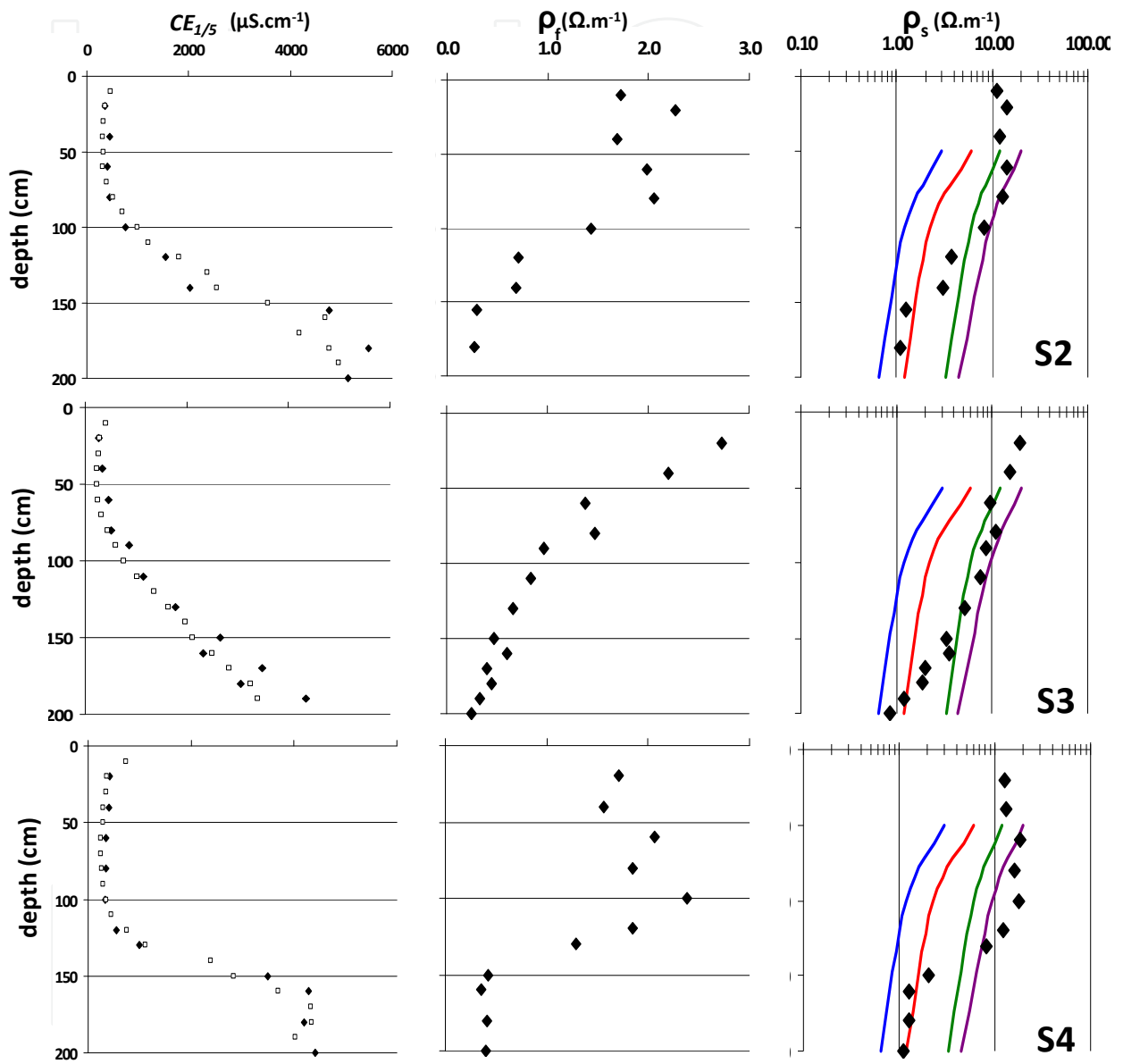
Fig. 12. Example of fluid resistivity (ρ_f) profile and soil resistivity (ρ_s) profiles calculated in the cornfield from the $CE_{1/5}$ and W profiles and using the Montoroi relation plus the Archie's law. The inverse calculated profiles show the vertical evolution of fluid salinity due to leaching in the upper unsaturated layer.
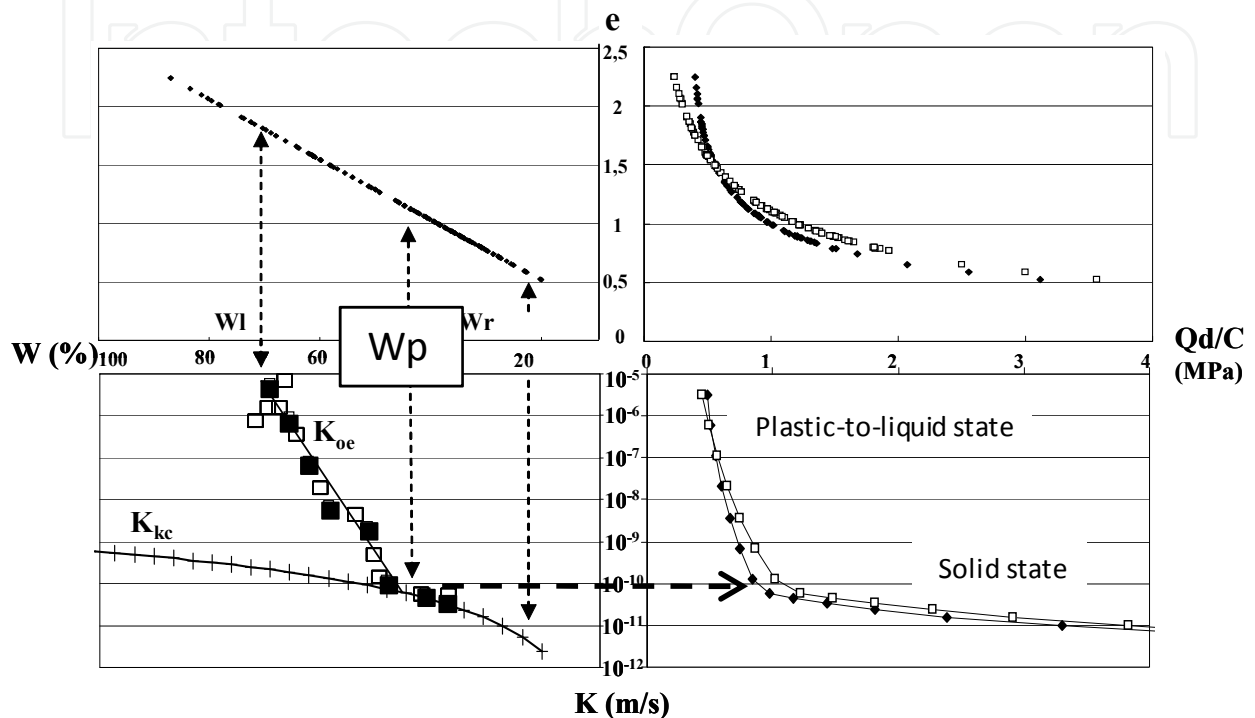
Fig. 13. Representation of the structure – hydro-mechanic properties of the marsh soils in the W-e-Qd/C-K crossed diagram. K = hydraulic conductivity, Kkc = hydraulic conductivity calculated from the clay matrix microstructure and Kozeny-Carman equation. Koe = conductivity hydraulic measured by oedometer compressivity test. The e - Qd/C curves are the average power laws characteristic of the desiccation profiles. The role of Wp is clearly shown in the Qd/C – K diagram by the differentiation of the two hydro-dynamical domains: i.e. solid state for W < Wp and plastic-to-liquid state for W>Wp.

The structure – hydro-mechanical relationship can be used to the explanation of the mechanism of soil structure behaviour (Figure 14).

These relationships based on the clay matrix shrinkage curve may be considered as dimensionless face to the hydro-mechanical behaviour of soil at the scale of the field via the geo-electrical section, at the scale of macroscopic samples from the prisms to the peds, and at the microscopic scale for particle arrangement along roots-soil contact for example (Figure 15).
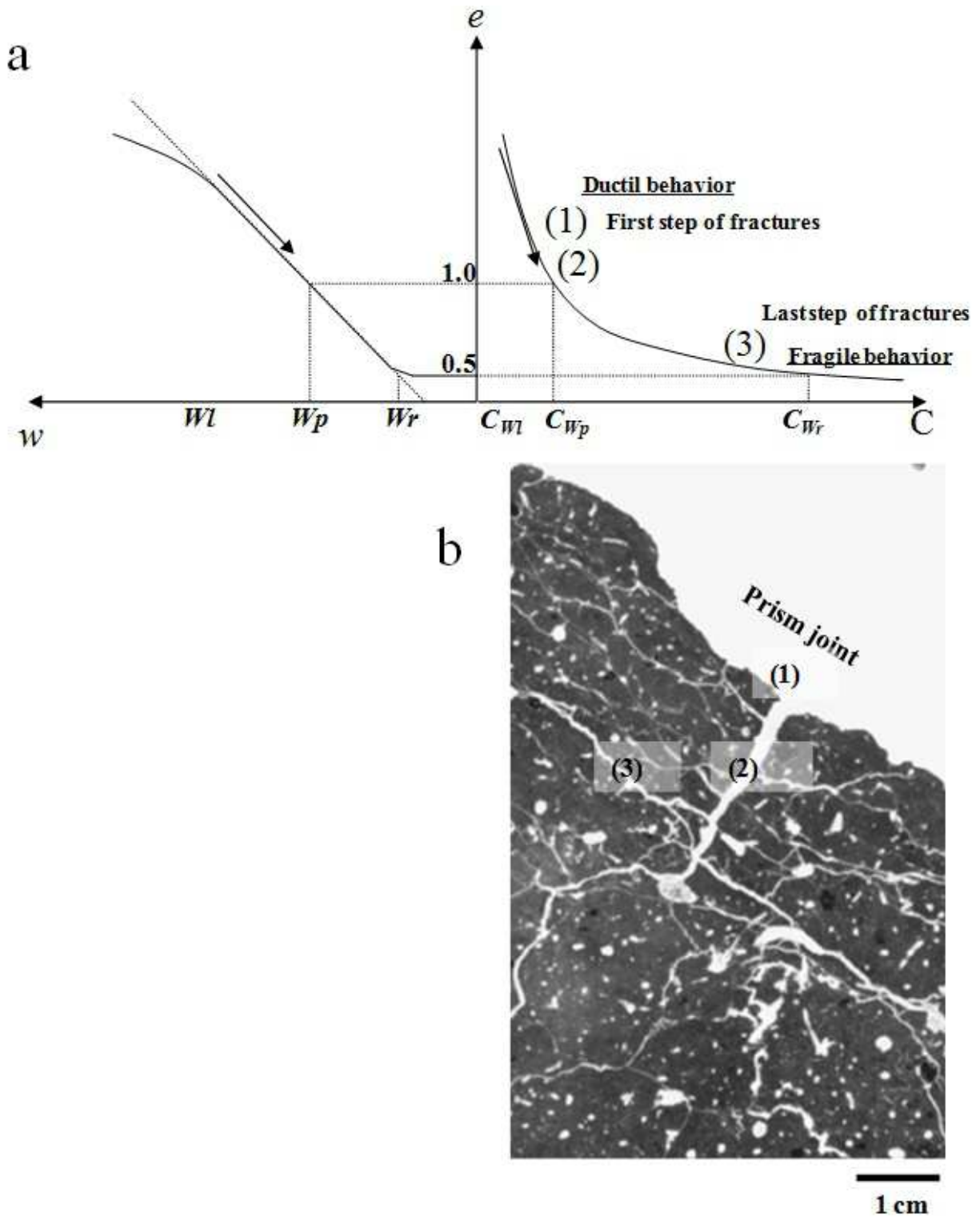
Fig. 14. a - Schematic representation of the ductile-to-fragile behaviour of the clay dominant soil taking into account the W-C couple evolution and successive steps of fracturing, b- result on the shrinkage fracture network observed on a polish section of a soil prism (grassland; from Dudoignon *et al.*, 2007 and Gallier, 2011). 1, 2 and 3 represent the successive steps of fracturing according to the shrinkage effect and increase of cohesion of the clay matrix which is associated to the desiccation effect.
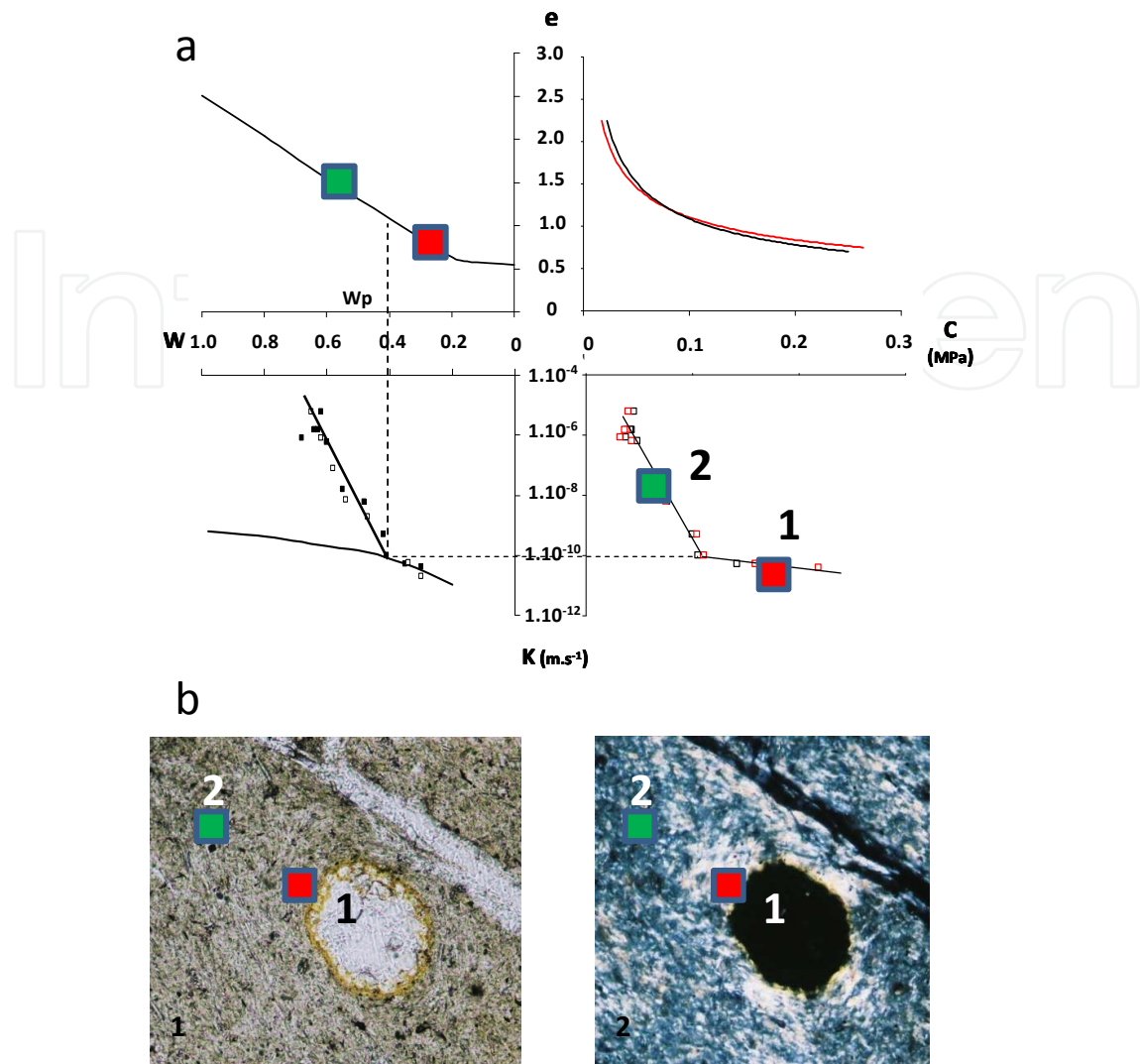
Fig. 15. Schematic representation of the hydromechanical behaviour of the soil clay matrix in a root environment. a and b - location of the 1 and 2 microsites in the root vicinity (b) and in the e-W-C-K diagram (a). 1: anisotropic and consolidated clay matrix along the root contact and 2 subisotropic and porous clay matrix 500 μm far away. The 1 and 2 microstructures of the clay matrix may be quantified by image analyses on polarized and analysed light (anisotropy) and by microanalysis on SEM (Dudoignon & Pantet, 1998; Dudoignon *et al.*, 2004).

5. Conclusion

The soil structure behaviour face to hydric of hydro-mechanic stress is governed by the facilities of the clay particles to rearrange (Biarez *et al.*, 1987; Dudoignon *et al.*, 2004). In fact the clay particle arrangement may be followed along the clay matrix shrinkage curve, thus it appears to be a good tool to make numerical relationship between the hydro-mechanical properties and structure of soil. The relationships may be described in W-e- mechanical resistance – hydraulic conductivity but also in W-e –resistivity crossed diagrams. Thus such works may be applied for modelling the soil structure behaviour for farming or geotechnic,

for modelling the shrinkage fracture network propagation introducing the cohesion in the mechanism. Finally, using the $CE_{1/5}$ and/or "*in situ*" resistivity profiles it can be aid for the modelling of hydric and salt stress in mashes territories (Gallier, 2011).

6. References

Archie, G. (1942). The electrical resistivity log as an aid in determining some reservoir characteristics. American Institute of Mining and Metallurgical Engineers, 154 pp. 1-8

Bernard, M. (2006). Etude des comportements des sols de marais: Evolution Minéralogique, Structurale et Hydromécanique. (Marai de Rochefort et Marais Poitevin). These de doctorat. Université e Poitiers. 309 p.

Bernard, M.; Dudoignon, P.; Pons, Y.; Chevallier, C. & Boulay, L. (2007). Structural characteristics of clay-dominant soils of a marsh and paleosol in a crossed diagram. European Journal of Soil Science, 58 (5) : pp. 1115-126

Bernard-Ubertosi, M.; Dudoignon, P. & Pons, Y. (2009). Characterization of structural profiles in clay-rich marsh soils by cone resistance and resistivity measurement. Soil Science Society of America Journal, 73 (1) : pp. 46-54

Biarez, J.; Fleureau, J-M. ; Zerhouni, M-I. & Soepandji, B.S. (1987). Variations de volume des sols argileux lors de cycles de drainage – humidification. Revue Française de Géotechnique, 41 : pp. 63-71

Braudeau, E.; Costantini, J-M.; Bellier, G. & Colleuille, H. (1999). New device and method for soil shrinkage curve measurement and characterization. Soil Science Society of America Journal, 63: pp. 525-535

Braudeau, E.; Frangy, J-P. & Mohtar R.H. (2004). Characterizing non rigid aggregated soil-water medium using its shrinkage curve. Soil Science Society of America Journal, 68: pp. 359-370

Brindley, G.W. & Brown, G. (1980). Crystal structures of clay minerals and their X-ray identification. London, Mineralogical Society.

Cassan, M. (1988). Les essais in situ en mécanique des sols-réalisation et interprétation. Eyrolles, pp. 146-151

Cornelis, W.M. ; Corluy, J.; Medina, H.; Diaz, J.; Hartmann, R.; Van Meirvenne, M. & Ruiz, M.E. (2006). Measuring and modeling the soil shrinkage characteristic curve. Geoderma, 137 (1-2): 179-191

Ducloux, J. (1989). Notice explicative de la carte pédologique de France au 1/100000 Fontenay-le-Conte. 16p.

Dudoignon, P. & Pantet, A. (1998). Measurement and cartography of clay matrix orientation by image analysis and grey-level diagram decomposition. Clay Minerals, 33 : pp. 629-642

Dudoignon, P.; Gelard, D. & Sammartino, S. (2004). Cam-clay and hydraulic conductivity diagram relations in consolidated and sheared clay-matrices. Clay Minerals, 39: pp. 269-279

Dudoignon, P.; Causseque, S.; Bernard, M.; Hallaire, V. & Pons, Y. (2007). Vertical porosity profile of a clay-rich marsh soil. Catena, 70 (3): pp. 480-492

Dudoignon, P.; Bernard-Ubertosi, M. & Hillaireau, J.M. (2009). Grasslands and coastal marshes management: role of soil structure. In grasslands, Ecology, management and restore. Nova Science Publishers (NY)

Gallier, J. (2011). Caracterisation des processus d'évolution structurale et de salinité es sols de marais côtiers par mesures mécaniques et géo-électriques in situ. Thèse de doctorat, Université de Poitiers, 218 p.

Grollier,J.; Fernadez, A.; Hucher, M. & Riss, J. (1991). Les propriétés physiques des roches : théories et modèles. Masson ed., Paris, 462 p.

Gourvés, R. & Barjot, R. (1995). The PANDA dynamic penetrometer , 11th Eurprean congress of soil mechanic and foundation works, Copenhague, pp.83-88

Langton, D.D. (1999). The Panda lightweight penetrometer for soil investigation and monitoring material compaction. Ground Engineering, 32 (9): pp. 33-37

Meunier, A. (2003). Argiles. Paris 433 p.

Mojid, M.A. & Cho, H. (2008). Wetting solution on an electrical double layer contribution to bulk electrical conductivity of sand-clay mixtures. Vadose Zone Journal, 7, pp. 992-980

Montoroi, J.P. (1997). Conductivité électrique de la solution du sol et d'extraits aqueux du sol – Application à un sol sulfaté acide salé de Bassa-Casamance (Sénégal). Etude et Gestion des sols, 4 pp. 279-298

Perdok, U.D.; Kroesbergen, B. & Hoogmoed, W.B. (2002). Possibilities for modelling the effect of compression on mechanical and physical properties of various Dutch soil types. Soil and Tillage Research, 65: pp. 61-75

Pons, Y. (1997). Comportements physiques et aptitudes à la mise en culture des sols des Marais de l'Ouest (Physica behavior and soil cropping possibilities of the French West Marshes), thèse de doctorat de l'Institut National Agronomique Paris – Grignon, 130 p.

Pons, Y. & Gerbaud, A. (2005). Classification agronomique des sols de marais à partir de la relation entre sodicité et stabilité structural. Application au cas des marais de l'ouest. Etude et gestion des sols, 12 (3) : pp. 229-244

Righi, D.; Velde, B. & Meunier, A. (1995). Clay stability in clay-dominated soil systems. Clay Minerals, 30 (1) : pp. 45-54

Tessier, D. & Pédro, G. (1984). L'organisation et le comportement des sols. Association Française d'Etude des Sols, livre Jubilaire, pp. 223-234

Tessier, D. ; Lajudie, A. & Petit, J-C. (1992). Relation between the macroscopic behaviour of clays and their microstructural properties. Applied Geochemistry, Supplement 1 (Supplementary Issue 1): pp. 151-161

Waxmann, M.H. & Smits, L.J.M.(1968). Electrical conductivities in oil-bearing shaly sands. Journal of Theo Society of Petroleum Engineering, 8, pp. 107- 120

Zhou, S. (1997). Caractérisation des sols de surface à l'aide du pénétromètre dynamique léger à energie varaible type „PANDA". Thèse de Doctorat. Université Blaise Pascal, Clermont Ferrand
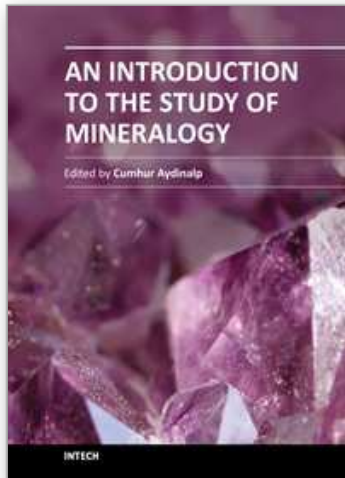
An Introduction to the Study of Mineralogy

Edited by Prof. Cumhur Aydinalp

An Introduction to the Study of Mineralogy is a collection of papers that can be easily understood by a wide variety of readers, whether they wish to use it in their work, or simply to extend their knowledge. It is unique in that it presents a broad view of the mineralogy field. The book is intended for chemists, physicists, engineers, and the students of geology, geophysics, and soil science, but it will also be invaluable to the more advanced students of mineralogy who are looking for a concise revision guide.

How to reference

In order to correctly reference this scholarly work, feel free to copy and paste the following:

J. Gallier, P. Dudoignon and J.-M. Hillaireau (2012). Microstructure – Hydro-Mechanical Property Relationship in Clay Dominant Soils, An Introduction to the Study of Mineralogy, Prof. Cumhur Aydinalp (Ed.), ISBN: 978-953-307-896-0, InTech, Available from: http://www.intechopen.com/books/an-introduction-to-the-study-of-mineralogy/microstructure-hydro-mechanical-property-relationship-in-clay-dominant-soils

INTECH
open science | open minds